

# Gold nanoparticles decorated with oligo(ethylene glycol) thiols: kinetics of colloid aggregation driven by depletion forces

Fajun Zhang · Donald G. Dressen · Maximilian W. A. Skoda ·  
Robert M. J. Jacobs · Stefan Zorn · Richard A. Martin · Christopher M. Martin ·  
Graham F. Clark · Frank Schreiber

Received: 29 September 2007 / Revised: 22 November 2007 / Accepted: 13 December 2007 / Published online: 9 January 2008  
© EBSA 2008

**Abstract** We have studied the kinetics of the phase-separation process of mixtures of colloid and protein in solutions by real-time UV–vis spectroscopy. Complementary small-angle X-ray scattering (SAXS) was employed to determine the structures involved. The colloids used are gold nanoparticles functionalized with protein resistant oligo(ethylene glycol) (OEG) thiol, HS(CH<sub>2</sub>)<sub>11</sub>(OCH<sub>2</sub>CH<sub>2</sub>)<sub>6</sub>OMe (EG6OMe). After mixing with protein solution above a critical concentration,  $c^*$ , SAXS measurements show that a scattering maximum appears after a short

induction time at  $q = 0.0322 \text{ \AA}^{-1}$ , which increases its intensity with time but the peak position does not change with time, protein concentration and salt addition. The peak corresponds to the distance of the nearest neighbor in the aggregates. The upturn of scattering intensities in the low  $q$ -range developed with time indicating the formation of aggregates. No Bragg peaks corresponding to the formation of colloidal crystallites could be observed before the clusters dropped out from the solution. The growth kinetics of aggregates is followed in detail by real-time UV–vis spectroscopy, using the flocculation parameter defined as the integral of the absorption in the range of 600–800 nm wavelengths. At low salt addition (<0.5 M), a kinetic crossover from reaction-limited cluster aggregation (RLCA) to diffusion-limited cluster aggregation (DLCA) growth model is observed, and interpreted as being due to the effective repulsive interaction barrier between colloids within the depletion potential. Above 0.5 M NaCl, the surface charge of proteins is screened significantly, and the repulsive potential barrier disappeared, thus the growth kinetics can be described by a DLCA model only.

Advanced neutron scattering and complementary techniques to study biological systems. Contributions from the meetings, “Neutrons in Biology”, STFC Rutherford Appleton Laboratory, Didcot, UK, 11–13 July and “Proteins At Work 2007”, Perugia, Italy, 28–30 May 2007.

F. Zhang · D. G. Dressen · M. W. A. Skoda · S. Zorn ·  
F. Schreiber (✉)  
Institut für Angewandte Physik, Universität Tübingen,  
Auf der Morgenstelle 10, 72076 Tübingen, Germany  
e-mail: frank.schreiber@uni-tuebingen.de

D. G. Dressen  
Department of Physics and Astronomy, University of Denver,  
2112 E. Wesley, Denver, CO 80208, USA

M. W. A. Skoda  
Physical and Theoretical Chemistry Laboratory,  
University of Oxford, South Parks Road, Oxford OX1 3QZ, UK

R. M. J. Jacobs  
Chemistry Research Laboratory, University of Oxford,  
12 Mansfield Road, Oxford OX1 3TA, UK

R. A. Martin  
School of Physical Sciences, Ingram Building,  
University of Kent, Canterbury CT2 7NH, UK

C. M. Martin · G. F. Clark  
SRS, Daresbury, Warrington, Cheshire WA4 4AD, UK

**Keywords** Gold nanoparticle ·  
Self-assembled monolayer · Protein resistance · SAXS ·  
UV–vis spectroscopy

## Introduction

The protein resistance of oligo(ethylene glycol) (OEG) self-assembled monolayers (SAMs) at liquid–solid interface has attracted much attention because of the numerous applications in biotechnology and medical devices (Ulman 1996; Mrksich and Whitesides 1996; Love et al. 2005; Schreiber 2000, 2004; Balamurugan et al. 2005; Herrwerth

et al. 2003; Kreuzer et al. 2003; Skoda et al. 2007). The majority of these studies have been performed on flat interfaces. However, there are many interesting applications of functionalized gold colloids that might benefit from tuning the surface properties using SAMs (Weisbecker et al. 1996; Zheng et al. 2003). In our previous work, we have studied the stability and protein resistance of OEG thiol coated gold colloids (Zhang et al. 2007b). It was found that OEG SAMs stabilize colloidal gold in solution in a wide range of temperature, ionic strength and pH. In addition, such OEG-protected gold colloids do not bind to protein indicating the protein resistance of the OEG SAM at curved interfaces.

One of the key observations from our previous study in this system is that the decorated colloids lose their stability and form aggregates upon adding protein above a critical concentration,  $c^*$  (Zhang et al. 2007b). Adding proteins to such a colloidal solution creates an attractive depletion interaction between colloids. This depletion effect is enhanced with increasing size of colloids due to the enhanced imbalance of osmotic pressure. A decrease of  $c^*$  was observed by using a larger size of colloid. The effective interaction between colloids also depends on the ionic strength of the solution as observed as the decrease of  $c^*$  upon increasing the ionic strength (Zhang et al. 2007a, b). This effect of ionic strength is explained as screening of the surface charge of proteins, which changes the interaction potential between colloids from a potential that can be described as “oscillatory” to a pure depletion attractive potential. In this work, we study the *kinetics* of phase separation of this effect using SAXS and real-time UV–vis spectroscopy.

The phase separation in a colloidal system with short-ranged attraction has become an attractive field, with implications for fundamental colloid science and cell biology as well as for industrial applications (Liu et al. 2005; Piazza 2000, 2004; Sedgwick et al. 2005; Stradner et al. 2004, 2005; Sear 2006). Phase separation in colloid–polymer and colloidal mixture systems has now been generally accepted as a depletion effect, i.e., the depletion effect leads to an unbalanced osmotic pressure pushing the large particles together, which results in an effective attraction between the two large particles (Anderson and Lekkerkerker 2002; Asakura and Oosawa 1954; Vrij 1976; Belloni 2000; Likos 2001; Poon 2002). The model systems in this area are binary colloid mixtures and colloid–polymer mixture. The former case is also called additive mixtures because the pair potential between the two species is described by their mean diameter, while in colloid–polymer mixtures, it is common to assume the polymer–polymer interactions are ideal so that the hard-sphere diameters are nonadditive (Dijkstra et al. 1999). A binary hard-sphere mixture with size asymmetry serves as the

model system to study depletion induced phase behavior. Dijkstra et al. (1999) have shown that the phase behavior of such a system can be accurately predicted by integrating out the effect of the small particles and introducing an effective depletion potential between the large particles. Experimentally, the equilibrium phase behavior of colloid–polymer mixtures has been reviewed by Poon (2002).

One of the most interesting phenomena associated with colloidal phase transition is the formation of long-lived metastable phases instead of the equilibrium phase. These kinetically locked-in phases show very rich possibilities due to the tunable interparticle potentials, and their intrinsically longer time scales (Sciortino and Tartaglia 2005; Renth et al. 2001). For example, Poon and Haw (1997) found that the nonequilibrium phase transition in colloid–polymer mixtures has three mechanisms: a nucleation-like behavior, a spinodal-like behavior, and transient gelation. Studies on depletion-driven colloidal aggregation kinetics on both experimentally and molecular dynamics simulations have revealed many interesting results. Hobbie (1998, 1999) investigated a binary colloidal mixture using video microscopy and found a two-stage crystallization process, i.e., the fluid–fluid phase separation occurred as an intermediate step. A kinetics crossover from power-law to stretched-exponential behavior was observed. This multi-step phase transition behavior via fluid–fluid transition was also observed in colloid–polymer systems at the triple point due to the “buried” metastable gas–liquid bimodal within the equilibrium fluid–crystal phase transition (Evans et al. 2001; Renth et al. 2001; Poon et al. 1999; Moussaïd et al. 1999). Using confocal scanning laser microscopy and small angle light scattering, Anderson et al. (2001) and de Hoog et al. (2001) studied the depletion-induced phase separation in a colloid–polymer mixture in real space. It was found that the kinetics and morphology of colloid aggregates strongly depends on the polymer concentration and both colloid crystals and amorphous sediments were observed. The mechanisms of the reaction limited cluster aggregation (RLCA), diffusion limited cluster aggregation (DLCA) and nucleation and growth were found to provide good descriptions of the phase separation regimes. Molecular dynamics simulations on the kinetics of depletion driven phase transition provided some interesting results. Cerdà et al. (2004) found that fractal clusters could be formed under strong attractive potential in the simulation. Interestingly, these fractal clusters have a hybrid structure, i.e., hexagonal closed-packed crystalline ordering at short length scales and a ramified fractal nature at larger length scales. For a sufficiently deep potential, the DLCA model dominates the kinetics process. A recent simulation of the aggregation kinetics of a highly asymmetric binary colloid mixture with short-range repulsive interactions shows that entropic inter-colloidal attractions (depletion effect) may induce the equilibrium phase fluctuation and result in the formation of

an amorphous cluster phase as observed in simulations (Bastea 2006).

Whereas most studies of the interactions and kinetics have been performed on systems which are, although already complex, simpler than that studied in this work. Here, by using UV–vis spectroscopy, we attempt to study the kinetics of functionalized nanoparticles together with proteins in aqueous solution, which is of significant importance for the behavior of nanoparticles in a biological environment, but obviously subject to rather complex interactions.

## Experimental section

### Materials

Citrate-stabilized gold colloids with mean size of 20 nm were purchased from British BioCell International (BBI) and were used as received. Hexa (ethylene glycol) terminated thiol,  $\text{HS}(\text{CH}_2)_{11}(\text{OCH}_2\text{CH}_2)_6\text{OMe}$ , was purchased from ProChimia, Poland and was used as received. Bovine serum albumin (BSA) (product no A7638) was purchased from Sigma-Aldrich. This is a lyophilized powder with a molecular weight of  $\sim 66$  kDa and was used as received.

### Preparation of surface-modified gold colloids

Monodispersed gold colloids were modified by directly adding 0.1 mg/mL EG6OMe to the colloid solution. This corresponds to an excess of EG6OMe by a factor between  $10^2$  and  $10^3$ , based on a simple calculation considering the total surface area of gold colloids and the cross-section of the thiol molecule. Weisbecker et al. (1996) reported detailed studies on the stability of various aliphatic thiols on gold colloids. They found that although alkanethiols with  $\text{HS}(\text{CH}_2)_n\text{R}$ ,  $\text{R} = \text{CH}_3$ ,  $\text{OH}$ , or  $\text{CO}_2\text{CH}_3$  lead to fast flocculation, oligo(ethylene glycol) thiols with  $\text{HS}(\text{CH}_2)_{11}(\text{OCH}_2\text{CH}_2)_y\text{OH}$ ,  $y > 3$ , stabilize the gold colloids. After the modified colloids were incubated at room temperature for more than 4 h, the stability of the modified colloids was examined by monitoring the UV–vis spectra when varying pH, ionic strength and temperature. The modified gold colloids are stable in the experimental conditions to temperature (5–70°C), NaCl concentration (0–1.0 M), and pH (1.3–12.4).

The colloidal solution is further concentrated up to 12 times by using a rotation-evaporation instrument under vacuum. For the following real-time UV–vis or SAXS studies, 0.05 mL concentrated colloid solution was mixed with 0.55 mL protein solution of various protein and salt concentration. In the final solution, the colloid has the same concentration as the original solution.

## Methods

### Real time UV–visible spectroscopy

Ultraviolet-visible absorption and kinetic measurements were performed at room temperature using a Cary 50 UV–visible spectrophotometer (Varian Optical Spectroscopy Instruments). Quartz or disposable PE UV cuvettes with an optical path length through the sample of 1.0 cm were used to contain the sample while collecting the spectra in the wavelength range from 300 to 800 nm. The concentrated colloid (0.05 mL) was quickly mixed with protein solution (0.55 mL) and then the real time UV–vis measurements were started immediately. It takes less than 1 min from mixing to starting the first scan.

### Small-angle X-ray scattering

Small-angle X-ray scattering (SAXS) measurements were carried out at station 6.2 of the Synchrotron Radiation Source (SRS) at the Daresbury Laboratory, Warrington UK (Cernik et al. 2004). The beam energy was 8.8 keV, corresponding to a wavelength of 1.51 Å. The scattered intensity was registered with a 200 mm-radius quadrant detector located 3.3 m from the sample. The accessible  $q$ -range was thus from 0.008 to  $0.25 \text{ \AA}^{-1}$ . The detector response was calibrated using the scattering from water. The angular scale was calibrated using the scattering peaks of Silver Behenate.

Protein and colloid solutions were filled into capillaries from Hilgenberg GmbH, Malsfeld, Germany. The capillaries are made of borosilicate glass with an inner diameter of 4.0 mm and a wall thickness of 0.05 mm. The scattering of water or a salt solution was measured as the background, in exactly the same way as the protein/colloidal solutions and was subtracted from the sample scattering. All measurements were carried out at room temperature. The resulting data were (electronically) converted to a 1D profile by integrating around an arc. The raw data were corrected for transmission, fluctuation of primary beam intensity, exposure time, and the geometry of the detector. The detailed data correction and calibration has been described in a previous publication (Zhang et al. 2007a, 2007b).

## Results and discussion

This section is organized as follows. First, we present the evolution of the structure of the aggregates in the early stage before dropping out by using real time SAXS measurements. This structural information provides the basis for the analysis of the kinetic UV–vis data. Second, we

present the central part of this study, i.e., the aggregation kinetics studied using UV–vis spectroscopy under different protein and salt concentrations. Last, we discuss the mechanisms of phase-separation kinetics by considering the various interactions in the mixtures.

#### Small-angle X-ray scattering observations and structure factor evolution

Figures 1 and 2 show the typical SAXS profiles of colloid/protein mixtures without and with salt addition, respectively, as a function of time. The critical protein concentration is around 380–400 mg/mL as determined in previous work (Zhang et al. 2007b). The SAXS profiles of Au20EG with 450 mg/mL BSA without salt added as a function of time are given in Fig. 1. After a short induction time (around 10 min), a sharp peak appears and develops with time at  $q = 0.0316 \text{ \AA}^{-1}$ , corresponding to a centre-to-centre distance of 200 Å. In the early stage (2 min), i.e., before the colloids strongly aggregated, the scattering profile of the mixture can be evaluated as the incoherent contribution for pure colloid solution and protein solution, very similar to the cases where protein concentration is lower than  $c^*$  as shown in previous work (Zhang et al. 2007b). The mean size and size distribution of several OEG thiol decorated gold colloid solutions have been studied in our previous publication (Zhang et al. 2007b). The Au20EG gold colloids used in this paper have a mean size of 188 Å. A comparison of the actual center-to-center distance of the nanoparticles within the aggregates of 200 Å (Fig. 1) demonstrates that the OEG thiol self-assembled monolayer is still on the surface of colloids as expected for the rather strong sulfur–gold bond. On the other hand, the aggregation is a reversible process, i.e., diluting the solution leads to dissolution of aggregates, which also proves that the SAMs are not destroyed during colloid aggregation process. Because of the very low volume fraction of gold colloid compared to protein in solution, the scattering of proteins in the mixture does not change with time or during the aggregation of colloid. This can be seen from the complete overlap of the scattering maximum at high  $q$ -range, which mainly corresponds to the scattering of protein. Therefore, the effective structure factor of the Au20EG can be evaluated by dividing the scattering intensity at time,  $t$ , i.e.,  $I(q, t)$  by the intensity at time equal to zero,  $I(q, 0)$ . Here, we use the first scattering profile taken about 2 min after mixing instead of the  $I(q, 0)$ , this is reasonable as long as the colloids are not aggregated significantly. The evaluated effective structure factor at different time has been plotted in Fig. 1b. Clearly, a peak corresponding to the interference of colloid with its nearest neighbor within the aggregates developed with time. It is

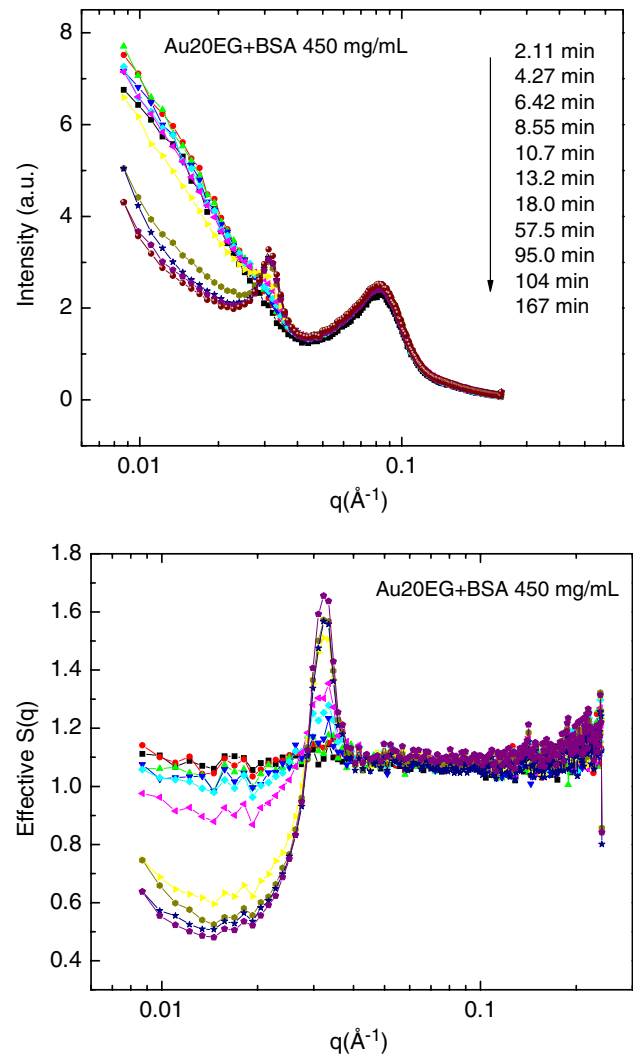


**Fig. 1** a Real time SAXS profiles of Au20EG with 450 mg/mL BSA; b effective structure factor  $S(q, t) = I(q, t)/I(q, t = 0)$  for SAXS data

interesting to see that the peak position does not change with time. Simultaneously, the structure factor in the low  $q$ -range decreases with time, but an upturn is observed in the very low  $q$ -range approaching the  $q = 0$ , which can be understood by the formation of colloid aggregates in the solutions. In the large  $q$ -range beyond the first maximum, there is no further minimum or second maximum developed with time. No other Bragg peaks indicating the formation of colloidal crystallites could be observed during the time period of the current experiments. These observations suggest that the colloid aggregates are in an amorphous phase instead of a crystalline phase as observed in many colloid/polymer systems upon aggregation.

Adding salt into the mixture speeds up the colloid aggregation dramatically. Figure 2a presents the Au20EG with 450 mg/mL BSA with 0.1 M NaCl. The correlation peak already appears even in the first scan (2 min). The effective structure factor in this case is evaluated by

dividing the intensity profiles (Fig. 2a) by the first profile in Fig. 1a. Note that the scattering profile of the very concentrated protein solution (450 mg/mL) changes only slightly on addition of 0.1 M NaCl in the low  $q$ -range. Therefore, we can still use the first profile in Fig. 1a to evaluate the effective structure factor in Fig. 2b, the error due to the slightly change of the intensity in the low  $q$ -range is less than 10%. A similar change was observed as shown in Fig. 1b. The peak position is exactly the same as in Fig. 1a and keeps constant but its intensity increases with time much faster. In the low  $q$ -range, the upturn at  $q$  approaching zero indicates the formation of aggregates. No other minima or maxima could be observed in the high  $q$ -range. Similar behavior has been observed for samples with different protein and salt concentrations (data not shown). The new peak appearing upon colloid aggregation

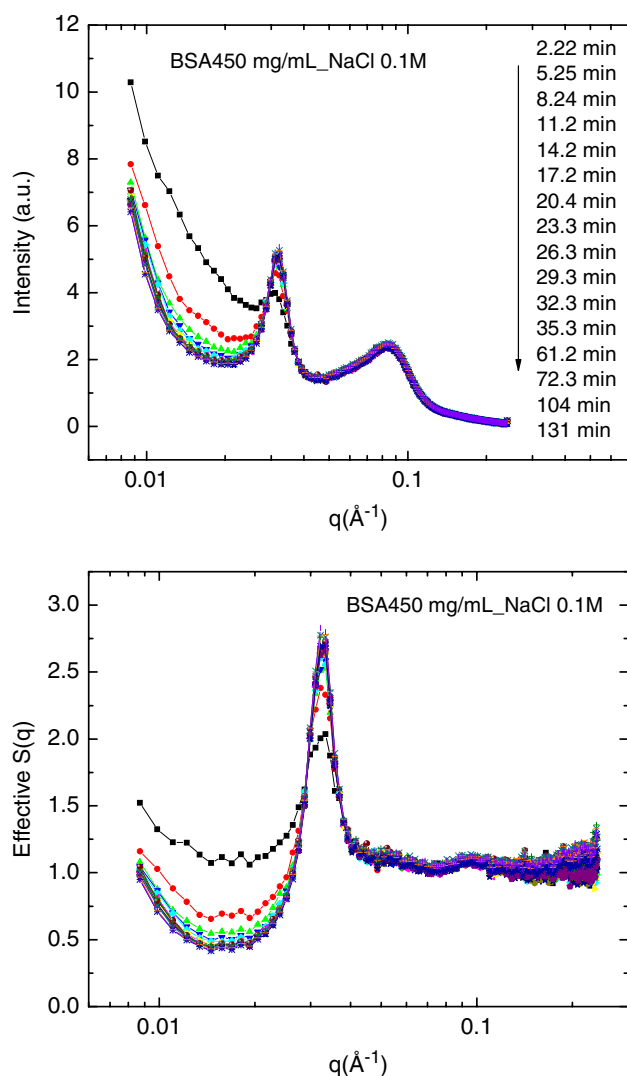


**Fig. 2** **a** Real time SAXS profiles of Au20EG with 450 mg/mL BSA with 0.1 M NaCl; **b** effective structure factor  $S(q, t) = I(q, t)/I(q, t = 0)$  for SAXS data

always has the same position and its intensity increase with time. Increasing protein concentration as well as salt concentration enhances the aggregate formation.

#### Ultraviolet–vis spectroscopy observations and data analysis

The growth kinetics of colloid aggregation driven by depletion force is mainly characterized by an empirical parameter, i.e., the flocculation parameter,  $P$ . This is used to compare the stability of thiol functionalized colloidal gold in solution under various ionic strength and pH conditions following the approach of Weisbecker et al. (1996). The flocculation parameter is defined as,

$$P = \int_{600}^{800} I_{\text{Abs}}(\lambda) d\lambda \quad (1)$$

It is the integral of absorption intensity between 600 and 800 nm. Theoretical modeling and comparison to TEM observations indicate that the formation of gold colloid aggregates result in additional resonances at wavelengths much longer than the adsorption bands exhibited by the isolated colloids. These resonances are concentrated above 600 nm in the visible spectrum (Weisbecker et al. 1996; Quinten and Kreibitz 1986).

Two models have been widely used to describe the aggregation process of colloidal particles in solutions (Meakin 1983, 1985; Meakin and Family 1987, 1988; Asnaghi et al. 1992; González 1993; Weitz et al. 1985; Di Biasio et al. 1994; Micali et al. 1998; Mallamace et al. 1999), namely reaction limited cluster aggregation (RLCA) and diffusion limited cluster aggregation (DLCA). The difference between the two models is essentially the differences in the sticking probability. The model of DLCA assumes that the colloids stick permanently as soon as they touch and thus the mechanism is limited by the time taken for particles to diffuse through the suspension and meet. The model of RLCA assumes that the particles do not stick to each other in the first contact; only a small fraction of encounters results in particles aggregation. Thus the aggregation is limited by the time taken to overcome an “energy barrier” which reduces the sticking probability from the first contact. These two models are characterized by the fractal dimension,  $D$ , the cluster size distribution and the mean cluster size as a function of time. It is found that  $D \sim 2.1$  and 1.8 for RLCA and DLCA, respectively (Weitz et al. 1985; Di Biasio et al. 1994; Micali et al. 1998; Mallamace et al. 1999). MD simulations and mean-field theoretical approaches based on the von Smoluchowski equation predict that the mean cluster size as a function of

time for RLCA gives an exponential growth as  $S(t) \sim \exp(t/k)$  and a power law growth for DLCA as  $S(t) \sim t^{1/D}$ . From the definition of the flocculation parameter, its time dependence,  $P(t)$ , might be related to the time dependent mean cluster size,  $S(t)$ , during colloid aggregation. We therefore, analyzed the data by fitting the flocculation parameter as a function of time using following equations.

$$\text{For DLCA : } P(t) \propto S(t) \propto t^\tau \quad (2)$$

$$\text{For RLCA : } P(t) \propto S(t) \propto \exp(t/k) \quad (3)$$

where  $\tau \sim 1/D$  is power index and  $k$  is a time constant. In order to compare the relative rate of colloid flocculation,  $t_{1/2}$ , the time necessary to reach the half maximum of the flocculation parameter increment,  $(P_{\max} - P_{\min})$ , is used to characterize the growth rate under various conditions.  $P_{\min} = 26.5$  is the flocculation parameter at  $t = 0$ , i.e., the integral of absorption intensity between 600 and 800 nm in wavelength before colloid aggregation.

In the case of colloid/protein mixture without salt added, the absorption peak decreases in intensity with time but the peak position is constant. The time dependence of the peak intensity may also shed light on the growth kinetics. However, in this case the monomer concentration is not the only part of the system that contributes to the peak. The formation of small clusters also gives a similar absorbance resonance to that of the monomers without significantly red-shifting the peak (Lazarides and Schatz 2000). Therefore, the data analysis on the growth kinetics is not straightforward. In the following, we study the aggregation kinetics using the time dependent flocculation parameter only because this is more reliable.

#### Effect of protein concentration

The colloid aggregation process has been followed by real time UV–vis spectroscopy for samples containing various BSA concentrations. Three of them are shown in Fig. 3. During the time evolution of the UV–vis spectrum a continual decay in the peaks' intensity as well as a simultaneous increase in the range of 600–800 nm wavelengths was observed. Our previous work has shown that the critical protein concentration,  $c^*$  for Au20EG6OMe is 380–400 mg/mL. In the 400 mg/mL BSA sample, slightly higher than  $c^*$  (Fig. 3a) the temporal evolution of the UV–vis spectrum was taken every 10 min for 600 min to allow the colloid to fully aggregate. Despite this, the final mixture is still a light pink, indicating only a partial colloid aggregation and precipitation. The UV–vis absorption spectrum was measured every minute for 120 min for the other samples (Fig. 3b, c). It is obvious that the decrease of peak intensity and the development of the absorption

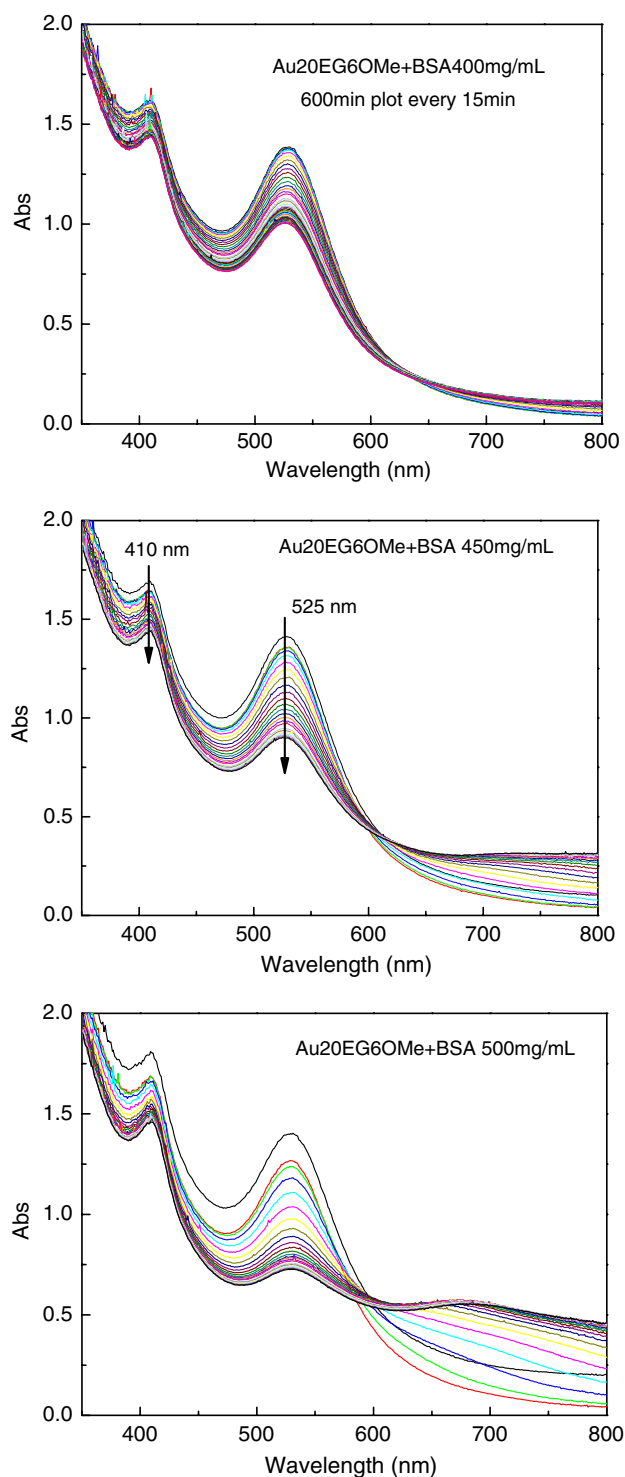


**Fig. 3** UV–vis spectra of Au20EG plus various protein concentrations as a function of time: **a** BSA 400 mg/mL measured every 10 min for 600 min; **b** BSA 450 mg/mL and **c** 500 mg/mL measured every 1 min for 120 min. The peak at 410 nm is because of the absorption of protein and the characteristic plasmon peak of colloidal gold appears at 525 nm wavelength. The plasmon peak does not shift, but peak intensity decreases with time, and the intensity between 600 and 800 nm increases at the same time

intensity in the high wavelength range are speeding up with increasing protein concentration. In order to see the early stage of the aggregation, a high time resolution scans for the sample with 450 mg/mL BSA was performed every 10 s for 120 min (data not shown).

The flocculation parameter is used to explore the mechanism of aggregation kinetics. Figure 4 shows the log–log plots of the temporal evolution of flocculation parameter for samples shown in Fig. 3. In the very early stage, as observed in the high time resolution scan for the sample with BSA 450 mg/mL, there is a clear exponential growth before 15 min and can be well-fitted by Eq. 3. This is in good agreement with the RLCA growth model. A power increase following the exponential increase has been observed as presented as a linear relation in the log–log plots (Fig. 4), which are the best fit by Eq. 2. The subsequent leveling off is due to the limited concentration for a given solution and a subsequent drop in the flocculation parameter occur after longer time. This drop in the flocculation parameter is due to the gold colloid clusters reaching a size where Brownian motion is no longer sufficient to keep them in solution, and sedimentation takes place. As a result these clusters precipitate out of solution and no longer contribute to resonances in the flocculation parameter region of the spectrum.

Table 1 shows fit parameters from Eqs. (2) and (3),  $t_{1/2}$ ,  $t_{\max}$  and  $P_{\max}$  are also listed in Table 1. From the value of  $t_{1/2}$  it is obvious that the growth rate increases with protein concentration. The  $t_{\max}$  follows the same tendency as  $t_{1/2}$ . The  $P_{\max}$  value increases with protein concentration

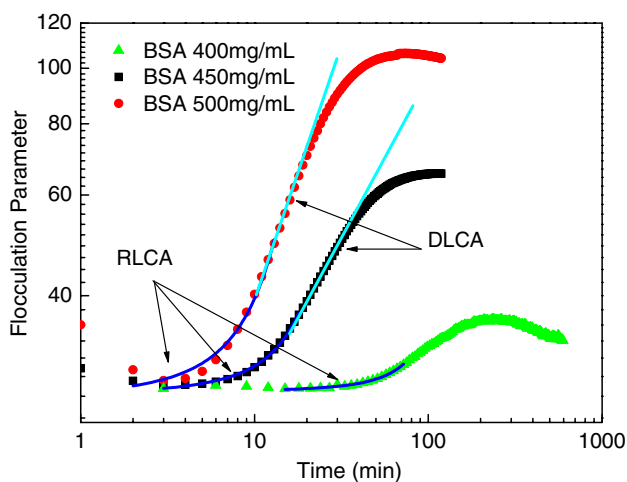


**Fig. 4** Log–log plots of flocculation parameter as a function of time, data for samples with 400 and 500 mg/mL BSA are from Fig. 3, data for sample with 450 mg/mL BSA is from high time resolution measurements. Data in the early stage was fitted by Eq. 2 (RLCA) and data in the intermediate stage was fitted by DLCA model. A crossover from RLCA to DLCA was observed

**Table 1** Fit results of aggregation kinetics

Sample	$k$ (min)	$\tau$	$P_{\max}$	$t_{\max}$ (min)	$t_{1/2}$ (min)
BSA400 mg/mL	$31 \pm 3$	–	36.3	210	87
BSA420 mg/mL	$17.6 \pm 0.9$	–	$\sim 40$	$\sim 120$	$\sim 61$
BSA450 mg/mL	$8.6 \pm 0.7$	0.52	65.4	111	27
BSA500 mg/mL	$5.8 \pm 0.9$	0.76	106	74	18
BSA550 mg/mL	–	0.86	136	59	17
BSA400 + NaCl 0.1 M	$13 \pm 2$	0.65	93.0	48	12
BSA400 + NaCl 0.5 M	–	0.90	133	21	5.5
BSA400 + NaCl 1.0 M	–	0.83	153	15	3.1
BSA400 + NaCl 2.0 M	–	–	156	34	1.5
BSA500 + NaCl 0.5 M	–	–	161	50	2.5
BSA500 + NaCl 1.0 M	–	–	158	71	2.0

Kinetics of aggregation of Au20EG6OMe with various protein and salt concentrations

indicating that more colloids aggregate during the time period of measurement. It therefore, may be related to the degree of aggregation upon increasing protein concentration. The RLCA time constant,  $k$ , was determined by fitting an exponential growth function to the time-evolution data of the flocculation parameter in the early stage. However, the very first few data points were neglected because they describe the system during a time of considerable inhomogeneity between the colloid and protein solution. The  $\tau$  value was determined through a linear fit of a log/log plot of the flocculation parameter as a function of time. Only data points that lay in the middle, linear portion of this plot were used to fit while the data at small and large time values were considered to be representative of RLCA aggregation and cluster precipitation, respectively. It is clear from the results listed in the table that increasing the concentration of BSA reduced the RLCA regime as  $k$  decreases, and the DLCA regime becomes dominant.

It is very interesting to see that the kinetics crossover with an initial short RLCA period followed by a longer period of DLCA can be clearly recognized for protein concentration less than 500 mg/mL. For a further increased protein concentration, the RLCA regime is too narrow to be distinguished because of the time resolution, sample preparation and also the inhomogeneity of the system in the early stage.

#### Effect of NaCl addition

Adding salt into the mixtures reduces the value of critical protein concentration,  $c^*$  dramatically as proved in our previous work (Zhang et al. 2007b). Up to 0.1 and 0.3 M

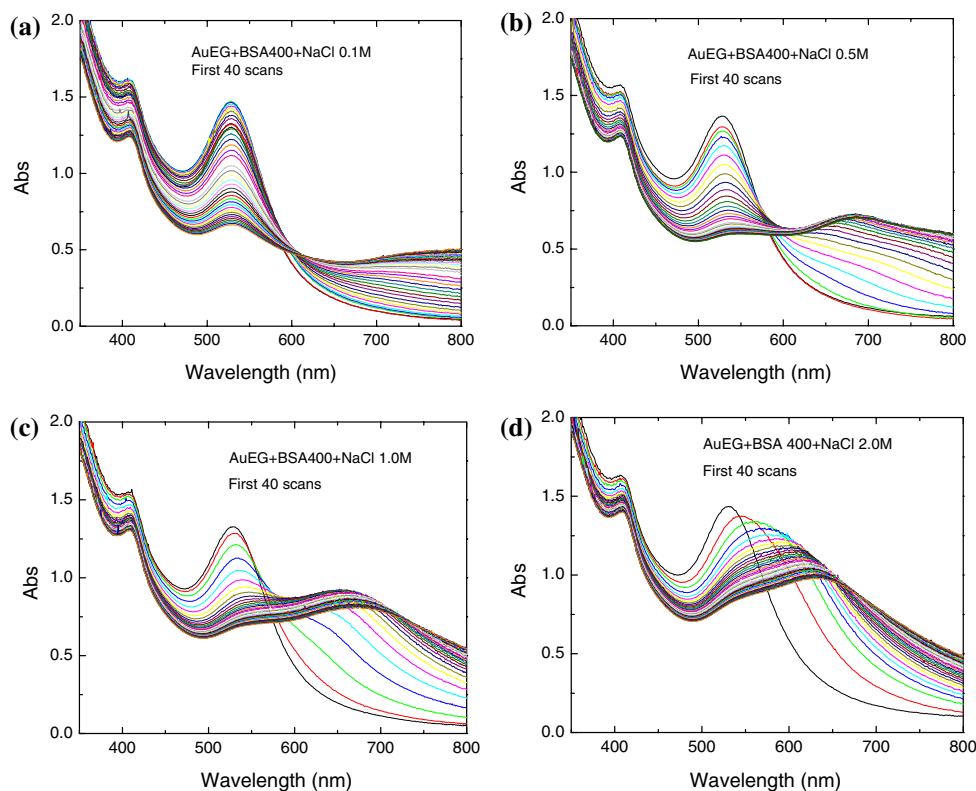
NaCl,  $c^*$  is reduced to 320 ~ 350, 280 ~ 310 mg/mL, respectively. The  $c^*$  does not change significantly upon further increasing the salt concentration above 0.5 M. The UV–vis results as well as direct observation on aggregation of colloidal gold upon salt addition are presented in Figs. 5, 6, 7. Four typical UV–vis spectra with samples containing a constant BSA concentration of 400 mg/mL and differing concentrations (0.1, 0.5, 1.0, and 2.0 M) of NaCl are presented in Fig. 5. The UV–vis absorption spectrum for the sample containing 0.1 M NaCl was taken every minute for 90 min, whereas for the sample containing 0.5 M NaCl the spectrum was measured every 10 s for 120 min in order to give detail at the early stage. In the 1.0 and 2.0 M NaCl samples aggregation occurred at a sufficiently rapid rate that the UV–vis absorption spectrum for each sample was measured every minute for a total of only 60 min. Qualitative comparison of the time evolution of the UV–vis spectral graphs shows an increase in the rate of growth of the flocculation parameter as NaCl is increased. A significant red-shift in the plasmon peak was also observed for the samples containing NaCl = 1.0, 2.0 M. The magnitude of the shift increased with increasing ionic strength.

Figure 6 shows a typical series of photographs for colloid aggregation of colloid solution with 500 mg/mL BSA plus 0.5 M NaCl in different stages. The first photo was taken right after the mixing; it looks pink without significant colloid aggregation. With increasing time, it becomes

darker indicating the aggregation of colloid. At a later stage, precipitation dominates and the solution becomes lighter. After 1 day, the color of the protein solution becomes light yellow. At the same time, a black precipitate could be observed at the bottom of the cuvette. It is worth noting here that the black precipitates could be redispersed by diluting the solution. Weisbecker et al. (1996) found that the blue or black precipitates in the bottom of a centrifuge tube could not usually be redispersed; red precipitates were easily redispersed.

Figure 7 presents the flocculation parameter data in the manner previously described from spectra in Fig. 5. The data for the 2.0 M NaCl sample was not fitted because the time resolution of the measurement was not precise enough to observe the aggregation mechanism. Fitting parameters as well as  $P_{\max}$  and  $t_{\max}$  were listed in Table 1. In the 0.1 M NaCl samples the early stage is evident by the exponential nature of the flocculation parameter data during the first 10 min of the scans (Fig. 7) indicating the existence of RLCA growth. For salt concentration higher than 0.5 M, only DLCA is possible. Crossover from an initial RLCA and a subsequent DLCA mechanism was seen in the samples where NaCl < 0.5 M. While  $P_{\max}$  is much larger and  $t_{1/2}$  is further reduced for samples with added salt compared to samples without salt,  $t_{\max}$  is no longer available to compare the relative growth rate. This is in agreement with our observation that adding salt enhances the colloid aggregation.

**Fig. 5** UV–vis spectra of Au20EG plus BSA 400 mg/mL with NaCl, **a–d** 0.1, 0.5, 1.0 and 2.0 M



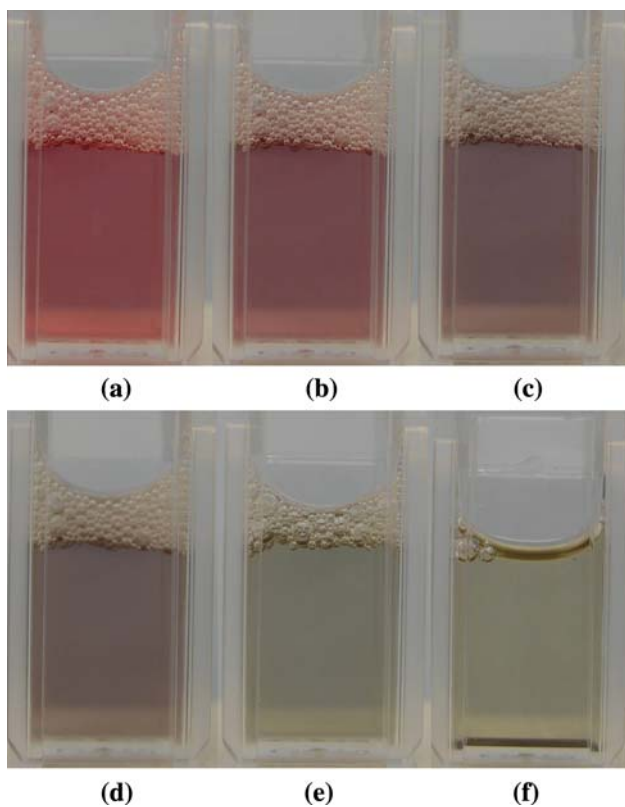


**Fig. 6** A series of photographs show the aggregation in a mixture of colloid plus 500 mg/mL BSA and NaCl 0.5 M at various times after mixing: a–f are 0.5, 1.5, 6, 15, 60 and 1,440 min, respectively

**Discussion of the relation between kinetic crossover and interactions in the mixture**

The simple one-step phase transition determined by SAXS is very important to understand our UV–vis observation. The transition from RLCA to DLCA observed for mixtures at low salt concentration is unlikely to be due to the formation of an intermediate phase. It is a pure kinetic crossover and can be understood by the effective interactions of protein–protein, protein–colloid and colloid–colloid in the mixture. From our previous work, we know that the effective interaction between colloids is an attraction rising from a depletion effect; the range of the potential depends on the interactions of both the BSA and coated colloid particles (Zhang et al. 2007b). Without salt addition, the effective potential between colloids can be described as an oscillation potential as illustrated in Fig. 8 (left). Since the decorated colloid particles are largely inert and the BSA molecules are negatively charged at neutral pH, the proteins tend to accumulate around the colloid particles as a way of minimizing the protein–protein repulsive interactions. The BSA molecules essentially impart a layer of partial negative charge density around the decorated colloid particles. On length scales greater than

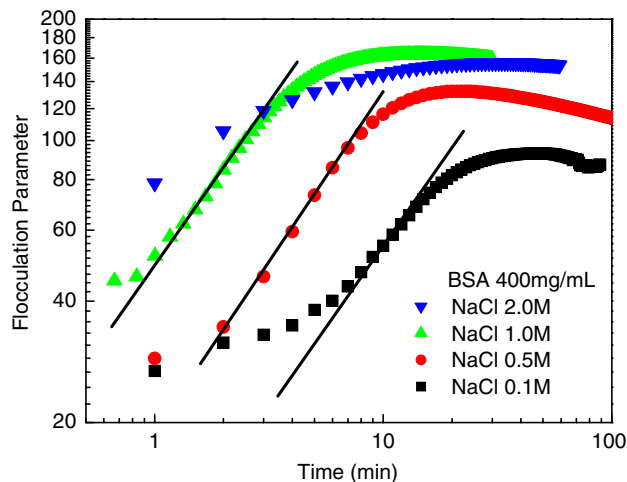


**Fig. 7** The log–log plots of flocculation parameter,  $P$ , as a function of time for data from Fig. 5. A crossover from RLCA to DLCA was observed for sample with low salt concentration (0.1 M)

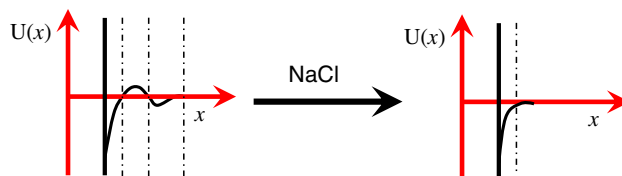


**Fig. 8** Schematic illustration on the effective interactions between functionalized gold colloids in colloid/protein mixtures without or with salt addition

the radius of interaction of the colloid–protein complex, a repulsive Coulombic force is created between colloid–protein complexes. This creates a potential barrier between colloids, which dramatically reduces the probability of collisions between colloidal that leads them sticking to each other, this results in a RLCA growth kinetics in the early stage. From this point of view, RLCA regime should exist for even high protein concentrations. In Table 1, for samples with BSA higher than 500 mg/mL, the growth is too fast to recognize the RLCA in the early stage because of the time resolution of UV–vis measurement and the sample preparation. With the size increase of aggregates, a crossover to DLCA occurs. The crossover can be understood both thermodynamically and dynamically (Di Biasio et al. 1994). Firstly, the attractive interaction potential due to the depletion effect between clusters continuously increases while the repulsion energy barrier does not change, therefore, for the larger colloid clusters, the interactions between clusters will be dominated by attraction. Secondly, the cluster–cluster aggregation is dependent on the probability of collisions that lead to aggregate formation. For isolated colloid the probability of sticking together after collision is low in spite of the relatively large diffusion coefficient. However, the clusters have a larger

sticking probability due to the larger relative energy of the impact overcoming a potential barrier.

Crossover in kinetics has been observed in many systems, for example the aggregation of the charge stabilized gold colloids. Upon a gradual substitution of the charge by Pyridin, a kinetics crossover from RLCA to DLCA was observed (Weitz et al. 1985). Combining UV–vis and elastic light scattering, Mallamace et al. (1999) studied the salt-induced aggregation kinetics of the porphyrin in solution. Their results suggested the presence of a RLCA regime in the early stage and a subsequent crossover to a DLCA regime (Micali et al. 1998). Di Biasio et al. (1994) performed a series of experiments of colloid aggregation in a suspension of polystyrene particles by adding NaCl. A kinetic crossover from exponential to power law was observed by varying the salt concentration. Further theoretical calculation based on the Smoluchowski equation allows a satisfactory interpretation of the experimental data.

Adding salt into the mixtures changes the effective interactions between proteins as well as the colloids. The long-range Coulombic repulsion between proteins is strongly reduced due to the screening effect of the salt and essentially returns the system to that of a simple hard-sphere model dominated primarily by attractive depletion forces between colloids as illustrated in Fig. 8 (right). This explained our experimental observations that adding salt increases the growth rate. This also explains why the initial RLCA growth process exists without salt addition but disappears at higher NaCl concentrations where a DLCA growth process dominates.

It should be noted that SAXS data show that at NaCl = 0.3 M, the surface charges are effectively screened (Zhang et al. 2007a). However, there is a continued increase in the rate of colloid aggregation in our system as NaCl increases above 0.3 M. The shielding effect alone of the NaCl is, therefore, insufficient in explaining this observation. The effect of high salt concentration on the viscosity of the solution is unlikely since the rheological measurements indicate that the shear viscosity of concentrated protein solution increases with salt concentration (Baglioni et al. 2004). The salt effects on the stability and kinetics are very complicated. Our further studies show salt nature dependence, similar to the “Hofmeister” effect. The details of these experiments are beyond the scope of the present paper and will be reported elsewhere (Zhang et al. 2008 in preparation).

## Conclusions

Based on our results and discussions presented above, we reach the following conclusions. SAXS measurements

confirmed that the depletion driven phase separation in the colloid–protein mixtures is a one-step process in our time window, forming an amorphous cluster phase. Increasing the protein concentration as well as salt addition increases the growth rate as characterized by the half time  $t_{1/2}$  for reaching the half maximum of the flocculation parameter. UV–vis observations show a kinetic crossover with low salt concentration from RLCA with exponential growth in the early stage to DLCA with power growth in the subsequent stage. The kinetic crossover is related to the interactions within the mixtures: the repulsive part of the effective oscillatory potential between colloids creates an energy barrier which initiates the RLCA growth in the early stage. Adding salt into the mixtures screens the surface charge of the proteins and the effective interactions between functionalized colloids becomes pure attraction, and the aggregation kinetics is dominated by DLCA only.

**Acknowledgments** We gratefully acknowledge financial support from the Engineering and Physical Sciences Research Council (EPSRC) and the CCLRC for the allocation of beamtime on MPW 6.2 at the SRS, Daresbury, UK. D. G. Dressen thanks the DAAD RISE Summer Program 2007.

## References

- Anderson VJ, de Hoog EHA, Lekkerkerker HNW (2001) Mechanisms of phase separation and aggregation in colloid-polymer mixtures. *Phys Rev E* 65:011403-1–011403-8
- Anderson VJ, Lekkerkerker HNW (2002) Insights into phase transition kinetics from colloid science. *Nature* 416:811–815
- Asakura S, Oosawa F (1954) On interaction between two bodies immersed in a solution of macromolecules. *J Chem Phys* 22:1255–1256
- Asnaghi D, Carpineti M, Giglio M, Sozzi M (1992) Coagulation kinetics and aggregate morphology in the intermediate regimes between diffusion-limited and reaction-limited cluster aggregation. *Phys Rev A* 45:1018–1023
- Baglioni P, Fratini E, Lonetti B, Chen SH (2004) Structural arrest in concentrated cytochrome C solutions: the effect of pH and salts. *J Phys Condens Matter* 16:S5003–S5022
- Balamurugan S, Ista LK, Yan J, López GP, Fick J, Himmelhaus M, Grunze M (2005) Reversible protein adsorption and bioadhesion on monolayers terminated with mixtures of oligo(ethylene glycol) and methyl groups. *J Am Chem Soc* 127:14548–14549
- Bastea S (2006) Aggregation kinetics in a model colloidal suspension. *Phys Rev Lett* 96:028305-1–4
- Belloni L (2000) Colloidal interactions. *J Phys Condens Matter* 12:R549–R587
- Cerdà JJ, Sintès T, Sorensen CM, Chakrabarti A (2004) Kinetics of phase transformations in depletion-driven colloids. *Phys Rev E Stat Nonlin Soft Matter Phys* E70:011405-1–011409
- Cernik RJ, Barnes P, Bushnell-Wye G, Dent AJ, Diakun GP, Flaherty JV, Greaves GN, Heeley EL, Helsby W, Jacques SDM, Kay J, Rayment T, Ryan A, Tang CC, Terrill NJ (2004) The new materials processing beamline at the SRS Daresbury, MPW6.2. *J Synchrotron Radiat* 11:163–170
- de Hoog EHA, Kegel WK, van Blaaderen A, Lekkerkerker HNW (2001) Direct observation of crystallization and aggregation in

- phase-separating colloid-polymer suspension. *Phys Rev E* 64: 021407-1–021407-9
- Di Biasio A, Bolle G, Cametti C, Codastefano P, Sciortino F, Tartaglia P (1994) Crossover region in the aggregation of colloids. *Phys Rev E Stat Phys Plasmas Fluids Relat Interdiscip Topics* 50:1649–1652
- Dijkstra M, van Roij R, Evans R (1999) Phase diagram of highly asymmetric binary hard-sphere mixtures. *Phys Rev E Stat Phys Plasmas Fluids Relat Interdiscip Topics* 59:5744–5771
- Evans RML, Poon WCP, Renth F (2001) Classification of ordering kinetics in three-phase systems. *Phys Rev E Stat Nonlin Soft Matter Phys* 64:031403-1–031403-13
- González AE (1993) Universality of colloid aggregation in the reaction limit: the computer simulations. *Phys Rev Lett* 71:2248–2251
- Herrwerth S, Eck W, Reinhardt S, Grunze M (2003) Factors that determine the protein resistance of oligoether self-assembled monolayers- internal hydrophilicity, terminal hydrophilicity, and lateral packing density. *J Am Chem Soc* 125:9359–9366
- Hobbie EK (1998) Metastability and depletion-driven aggregation. *Phys Rev Lett* 81:3996–3999
- Hobbie EK (1999) Depletion-driven phase separation and reversible aggregation in confined colloidal mixtures. *Langmuir* 15:8807–8812
- Kreuzer HJ, Wang RLC, Grunze M (2003) Hydroxide ion adsorption on self-assembled monolayers. *J Am Chem Soc* 125:8384–8389
- Lazarides AA, Schatz GC (2000) DNA-linked metal nanopore materials: structure basis for the optical properties. *J Phys Chem B* 104:460–467
- Likos CN (2001) Effective interactions in soft condensed matter physics. *Phys Rep* 348:267–439
- Liu Y, Fratini E, Baglioni P, Chen WR, Chen SH (2005) Effective long-range attraction between protein molecules in solutions studied by small angle neutron scattering. *Phys Rev Lett* 95:118102-1
- Love JC, Estroff LA, Kriebel JK, Nuzzo RG, Whitesides GM (2005) Self-assembled monolayers of thiolates on metals as a form of nanotechnology. *Chem Rev* 105:1103–1169
- Mallamace F, Monsu'Scolaro L, Romeo A, Micali N (1999) Crossover in the kinetics growth process of porphyrin aggregation. *Phys Rev Lett* 82:3480–3483
- Meakin P (1983) Formation of fractal clusters and networks by irreversible diffusion-limited aggregation. *Phys Rev Lett* 51:1119–1122
- Meakin P (1985) Dynamic cluster-size distribution in cluster-cluster aggregation: effect of cluster diffusivity. *Phys Rev B* 31:564–569
- Meakin P, Family F (1987) Structure and dynamics of reaction-limited aggregation. *Phys Rev A* 36:5498–5501
- Meakin P, Family F (1988) Structure and kinetics of reaction-limited aggregation. *Phys Rev A* 38:2110–2123
- Micali N, Monsu'Scolaro L, Romeo A, Mallamace F (1998) Light absorption study of aggregation porphyrin in aqueous solutions. *Phys Rev E* 57:5766–5770
- Moussaïd A, Poon WCK, Pusey PN, Soliva MF (1999) Structure of marginal and fully developed colloidal liquids. *Phys Rev Lett* 82:225–228
- Mrksich M, Whitesides GM (1996) Using self-assembled monolayers to understand the interreactions of man-made surfaces with proteins and cells. *Annu Rev Biophys Biomol Struct* 25:55–78
- Piazza R (2000) Interactions and phase transitions in protein solutions. *Curr Opin Colloid Interface Sci* 5:38–43
- Piazza R (2004) Protein interactions and association: an open challenge for colloid science. *Curr Opin Colloid Interface Sci* 8:515–522
- Poon WCP (2002) The physics of a model colloid-polymer mixture. *J Phys Condens Matter* 14:R859–R880
- Poon WCP, Haw MD (1997) Mesoscopic structure formation in colloidal aggregation and gelation. *Adv Colloid Interface Sci* 73:71–126
- Poon WCP, Renth F, Evans RML, Fairhurst DJ, Cates ME, Pusey PN (1999) Colloid-polymer mixtures at triple coexistence: kinetic maps from free-energy landscapes. *Phys Rev Lett* 83: 1239–1242
- Quinten M, Kreibitz U (1986) Optical properties of aggregates of small metal particles. *Surf Sci* 172:557–577
- Renth F, Poon WCK, Evans RML (2001) Phase transition kinetics in colloid-polymer mixtures at triple coexistence: kinetics maps from free-energy landscapes. *Phys Rev E Stat Nonlin Soft Matter Phys* 64:031402-1–031409
- Schreiber F (2000) Structure and growth of self-assembling monolayers. *Prog Surf Sci* 65:151–256
- Schreiber F (2004) Self-assembled monolayers: from 'simple' model systems to biofunctionalized interfaces. *J Phys Condens Matter* 16:R881–R900
- Sciortino F, Tartaglia P (2005) Glassy colloidal systems. *Adv Phys* 54:471–524
- Sear RP (2006) Interactions in protein solutions. *Curr Opin Colloid Interface Sci* 11:35–39
- Sedgwick H, Kroy K, Salonen A, Robertson MB, Egelhaaf SU, Poon WCK (2005) Non-equilibrium behaviour of sticky colloidal particles: beads, clusters and gels. *Eur Phys J E Soft Matter* 16:77–80
- Skoda MWA, Jacobs RMJ, Willis J, Schreiber F (2007) Hydration of oligo(ethylene glycol) self-assembled monolayers studied using polarization modulation infrared spectroscopy. *Langmuir* 23:970–974
- Stradner A, Sedgwick H, Cardinaux F, Poon WCK, Egelhaaf SU, Schurtenberger P (2004) Equilibrium cluster formation in concentrated protein solutions and colloids. *Nature* 432:492–495
- Stradner A, Thurston GM, Schurtenberger P (2005) Tuning short-range interactions in protein solutions: from attractive glasses to equilibrium clusters. *J Phys Condens Matter* 17:S2805–S2816
- Ulman A (1996) Formation and structure of self-assembled monolayers. *Chem Rev* 96:1533–1554
- Vrij A (1976) Polymers at interfaces and the interactions in colloidal dispersions. *Pure Appl Chem* 48: 471–483
- Weisbecker CS, Merritt MV, Whitesides GM (1996) Molecular self-assembly of aliphatic thiols on gold colloids. *Langmuir* 12:3763–3772
- Weitz DA, Huang JS, Lin MY, Sung J (1985) Limits of the fractal dimension for irreversible kinetic aggregation of gold colloids. *Phys Rev Lett* 54:1416–1419
- Zhang F, Skoda MWA, Jacobs RMJ, Martin RA, Martin CM, Schreiber F (2007a) Protein interactions studied by SAXS: effect of ionic strength and protein concentration for BSA in aqueous solutions. *J Phys Chem B* 111:251–259
- Zhang F, Skoda MWA, Jacobs RMJ, Zorn S, Martin RA, Martin CM, Clark GF, Goerigk G, Schreiber F (2007b) Gold nanoparticles decorated with oligo(ethylene glycol) thiols: protein resistance and colloidal stability. *J Phys Chem A* doi:10.1021/jp074293v
- Zhang F, Dressen DG, Skoda MWA, Jacobs RMJ, Zorn S, Martin RA, Martin CM, Clark GF, Schreiber F (2008) Gold nanoparticles decorated with oligo(ethylene glycol) thiols: Effect of salt nature on colloidal stability (in preparation)
- Zheng M, Davidson F, Huang X (2003) Ethylene glycol monolayer protected nanoparticles for eliminating nonspecific binding with biological molecules. *J Am Chem Soc* 125:7790–7791